Magnon spectra and strong spin-lattice coupling in magnetically frustrated MnB_2O_4 (B = Mn,V): Inelastic light-scattering studies

S. L. Gleason,[1,*] T. Byrum,[1,*] Y. Gim,[1] A. Thaler,[1] P. Abbamonte,[1] G. J. MacDougall,[1] L. W. Martin,[2]
H. D. Zhou,[3,4] and S. L. Cooper[1]

[1]*Department of Physics and Materials Research Laboratory, University of Illinois, Urbana, Illinois 61801, USA*

[2]*Department of Materials Science and Engineering and Materials Research Laboratory, University of Illinois, Urbana, Illinois 61801, USA*

[3]*Department of Physics and Astronomy, University of Tennessee, Knoxville, Tennessee 37996-1200, USA*

[4]*National High Magnetic Field Laboratory, Florida State University, Tallahassee, Florida 32306-4005, USA*

The ferrimagnetic spinels MnB_2O_4 (B = Mn,V) exhibit a similar series of closely spaced magnetic and structural phase transitions at low temperatures, reflecting both magnetic frustration and a strong coupling between the spin and lattice degrees of freedom. Careful studies of excitations in MnB_2O_4 (B = Mn,V), and the evolution of these excitations with temperature, are important for obtaining a microscopic description of the role that magnetic excitations and spin-lattice coupling play in the low-temperature phase transitions of these materials. We report an inelastic light (Raman) scattering study of the temperature and magnetic-field dependences of one- and two-magnon excitations in MnV_2O_4 and Mn_3O_4. We observe a pair of $\mathbf{q} = 0$ one-magnon modes at 74 and 81 cm^{-1} in MnV_2O_4, which is in contrast with the single 80-cm^{-1} $\mathbf{q} = 0$ magnon that has been reported for MnV_2O_4 based on previous neutron-scattering measurements and spin-wave calculations. Additionally, we find that the two-magnon energy of MnV_2O_4 decreases ("softens") with decreasing temperature below T_N, which we attribute to strong coupling between magnetic and vibrational excitations near the zone boundary.

PACS number(s): 78.30.−j, 75.30.Ds, 75.47.Lx, 75.30.Kz

I. INTRODUCTION

Spinel compounds (chemical formula AB_2X_4) consist of an A-site diamond sublattice and a geometrically frustrated B-site pyrochlore sublattice [1]. A remarkable feature of these materials is the diversity of phenomena that result from the substitution of magnetic ions on the frustrated B-site sublattice. For example, superconductivity [2], charge ordering [3], and heavy fermion behavior [4] have all been reported in the LiB_2O_4 (B = Ti,Mn,V) family of spinels. The ferrimagnetic spinels Mn_3O_4 [5–7] and MnV_2O_4 [7–10] offer a particularly interesting comparison: Both systems exhibit a similar series of closely spaced magnetic and structural phase transitions at low temperatures, reflecting both magnetic frustration and a strong coupling between the spin and lattice degrees of freedom. For example, MnV_2O_4 orders ferrimagnetically below $T_N = 56$ K but transitions to a noncollinear ferrimagnetic phase following a cubic-to-tetragonal structural transition at $T_o = 53$ K [7–10]. Similarly, Mn_3O_4 orders in a noncollinear ferrimagnetic phase below $T_N = 42$ K before subsequently transitioning first to an incommensurate magnetic phase at $T_1 = 39$ K, and then to a cell-doubled version of the noncollinear ferrimagnetic phase below a tetragonal-to-orthorhombic structural transition at $T_2 = 33$ K [5,6]. It remains an open question how these complex magnetostructural transitions in MnB_2O_4 (B = Mn,V) are influenced by the orbital configurations, which are quite different in Mn_3O_4 and MnV_2O_4. While the B-site Mn^{3+} ion in Mn_3O_4 is locked into a specific orbital configuration[1] below the cubic-to-tetragonal transition near

$T_o = 1440$ K [5–7,11], the B-site V^{3+} ion in MnV_2O_4 remains orbitally degenerate below the cubic-to-tetragonal structural transition at 53 K [7,10,12]. Various orbital configurations for the V^{3+} ion in MnV_2O_4 have been proposed, including alternating d_{xz} and d_{yz} orbitals ($L = 0$) along the c axis [13], a complex $d_{xz}+id_{yz}$ ($L = 1$) configuration [14,15], and even more complicated mixtures of d-orbital states [16–19].

Careful studies of excitations in MnB_2O_4 (B = Mn,V), and the evolution of these excitations with temperature, are important for obtaining a microscopic description of the role that magnetic excitations and spin-lattice coupling play in the low-temperature phase transitions of these materials. To date, however, there has been little study of the temperature-dependent evolution of the magnetic excitations in MnV_2O_4 and Mn_3O_4. In this paper, we report an inelastic light (Raman) scattering study of the temperature and magnetic-field dependences of one- and two-magnon excitations in MnV_2O_4 and Mn_3O_4. We show that while the two-magnon energy of Mn_3O_4 has a conventional temperature dependence the two-magnon energy of MnV_2O_4 exhibits an anomalous decrease ("softening") with decreasing temperature below T_N, which we attribute to strong spin-lattice coupling associated with zone-boundary magnons in MnV_2O_4. In addition, our high-resolution study of MnV_2O_4 at $T = 3$ K reveals a $\mathbf{q} = 0$ one-magnon spectrum that differs in important respects from previous neutron-scattering results and spin-wave calculations.

---

*These authors contributed equally to this work.

[1]Specifically, in the high-temperature cubic phase ($T > 1443$ K), the Mn^{3+} ($3d^4$) ions on the B sites of Mn_3O_4 have filled t_{2g} levels

and a single electron occupying the twofold degenerate e_g levels. However, the twofold orbital degeneracy of the e_g states is lifted by a cooperative Jahn-Teller distortion involving a c-axis lattice expansion at $T_{JT} = 1443$ K, which is associated with $d_{3z^2-r^2}$ ferro-orbital order.

II. EXPERIMENT

A. Sample preparation

Single-crystal samples of MnV_2O_4 were grown at Florida State University using a traveling-solvent-floating-zone technique [8]. The feed and seed rods for the crystal growth were prepared by solid-state reaction. Appropriate mixtures of MnO and V_2O_3 were ground together and pressed into 6-mm-diameter, 60-mm-long rods under 400 atm hydrostatic pressure, and then calcined in vacuum in a sealed quartz tube at 950 °C for 12 h. The crystal growth was carried out in argon gas in an NEC infrared-heated image furnace equipped with two halogen lamps and double ellipsoidal mirrors. The growth was conducted with the feed and seed rods rotating in opposite directions at 25 rpm during crystal growth at a rate of 30 mm/h. Because of the evaporation of V_2O_3 during the growth, extra V_2O_3 in the starting material and high growth speeds are critical for obtaining high-quality samples. The structural and magnetic properties of the resulting crystal are reported elsewhere [8]. The crystal exhibits two magnetic transitions at 56 and 52 K [8], consistent with previously reported temperatures [7,9,10].

Single-crystal samples of Mn_3O_4 were grown at the University of Illinois using a floating-zone technique [20,21]. Commercially available fine Mn_3O_4 powder [manganese (II, III) oxide, $\sim$325 mesh, 97%, Sigma-Aldrich Co.] was used as the starting material. The powder was formed into feed and seed rods with a diameter of 10 mm and a length of 150 mm and was pressed at a hydrostatic pressure of 400 atm. The pressed rods were sintered at 1050 °C for 5 h with an argon gas flow of 0.5 L/min. Single-crystal growth was performed using a four-ellipsoid-mirror furnace (Crystal Systems, Inc., FZ-T-10000-H-VI-VP) equipped with four 1000-W halogen lamps. The growth used a feed and seed (upper and lower shaft) rotation rate of 35 rpm in opposite directions, a growth rate (mirror-stage moving rate) of 5 mm/h, a feeding rate (upper-shaft moving rate) of 1 mm/h, and a growth atmosphere of oxygen at a gas pressure of 1 atm. The structural and magnetic properties of the resulting crystal are reported elsewhere [20–22]. The crystal exhibits three magnetic transitions at 43, 39, and 33 K, consistent with previously reported temperatures [5,6].

The crystallographic orientations of the samples used in this experiment were determined via x-ray diffraction performed at room temperature.

B. Raman-scattering measurements

Raman-scattering measurements were performed using the 647.1-nm excitation line from a Kr^+ laser. The incident laser power was limited to 10 mW and was focused to a $\sim$50-μm diameter spot to minimize laser heating of the sample, which was estimated to be roughly 4 K. The scattered light from the samples was collected in a backscattering geometry, dispersed through a triple stage spectrometer, and then detected with a liquid-nitrogen-cooled CCD detector. The samples were inserted into a continuous He-flow cryostat, which was horizontally mounted in the open bore of a superconducting magnet, allowing Raman measurements while the temperature

was varied in the range $T = 3$–290 K and the magnetic field was varied in the range $H = 0$–8 T.

For the scattering experiments involving Mn_3O_4, the incident light was circularly polarized with wave vector **k** parallel to the c axis. No analyzer was employed, in order to couple to as many components of the Raman tensor as possible in this geometry. The magnetic field used in the magnetic-field dependent measurements was directed along the c axis, parallel to **k**. For the scattering experiments involving MnV_2O_4, two experimental geometries were used. In geometry 1, the incident light was circularly polarized with **k** parallel to a cubic axis. No analyzer was employed, in order to couple to as many components of the Raman tensor as possible in this geometry. The magnetic field used in the magnetic-field dependent measurements was directed along the same cubic axis, parallel to **k**. In geometry 2, a 1-T magnetic field was applied to define a unique [001] crystallographic direction in the sample,[2] where [hkl] refer to tetragonal axes. The incident light was linearly polarized along $[11\sqrt{2}]$ with $\mathbf{k} \parallel [1\bar{1}0]$. An analyzer was employed to match the scattered polarization with the incident polarization along $[11\sqrt{2}]$. This geometry was used to equalize the intensities of the one-magnon excitations observed in MnV_2O_4 [see Fig. 1(d)].

III. RESULTS

Figure 1 shows the temperature dependence of the MnV_2O_4 Raman spectrum in the 40–240-cm^{-1} energy range, which is expected to be dominated by magnon excitations [7]. The higher-frequency phonon spectrum we observe in MnV_2O_4 is consistent with that reported previously [23] and will not be reproduced here.[3] For temperatures near and above T_N, the Raman spectrum of MnV_2O_4 exhibits a broad continuum background. Since MnV_2O_4 is insulating [24], it is unlikely that this continuum background represents inelastic electronic scattering. Rather, we associate this background with incoherent spin scattering similar to that observed in Raman scattering from low-dimensional spin systems [25] and Cr-based spinels [26]. For temperatures $T < T_N$, this incoherent spin scattering is suppressed, and several peaks develop, including two sharp modes at 74 cm^{-1} (M1) and 81 cm^{-1} (M2), a broad mode centered at 178 cm^{-1} (2M), and a weak "shoulder" near 90 cm^{-1} that will be discussed in more detail in a later publication.

We identify the narrow peaks M1 and M2 as $\mathbf{q} = 0$ one-magnon excitations, based upon the following: Both peaks broaden and decrease in energy as $T \to T_N$, tracking the sublattice magnetization, and are absent at temperatures above T_N. Additionally, as shown in Fig. 2, the energies of M1 and M2 change linearly with increasing magnetic field applied along the net magnetization direction—with rates of
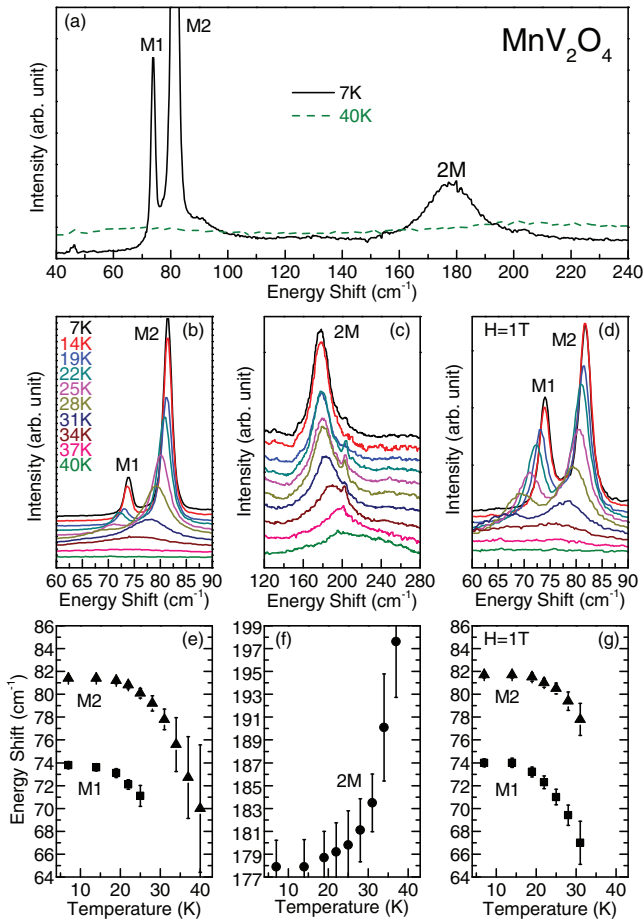

FIG. 1. (Color) (a)–(c) Raman-scattering spectra of MnV_2O_4 taken in geometry 1 (see discussion in Sec. II B) at various temperatures in the energy ranges (a) 40–240 cm^{-1}, (b) 60–90 cm^{-1}, and (c) 120–280 cm^{-1}. (d) Raman-scattering spectra of MnV_2O_4 taken in geometry 2 (see discussion in Sec. II B) at various temperatures in the energy range 60–90 cm^{-1}. The data in (b)–(d) have been offset for clarity. (e)–(g) Summaries of the temperature dependences of the peak positions for peaks labeled M1, M2, and 2M, as estimated by eye.

$\Delta E/\Delta H = +0.75$ and $+0.33$ cm^{-1}/T, respectively—consistent with the field dependence expected of one-magnon excitations [27]. Finally, previous inelastic neutron-scattering measurements of MnV_2O_4 confirm that there are magnon branches very close in energy to M1 (74 cm^{-1}) and M2 (81 cm^{-1}): One neutron study reports a $\mathbf{q} = 0$ one-magnon band near 80 cm^{-1} [7], while a second study reports the crossing of two one-magnon bands near 80 cm^{-1} at $\mathbf{q} = 0$ [28].

The broad two-magnon band 2M in Fig. 1 was previously observed in Raman-scattering measurements and was attributed to one-magnon scattering [23,29]. Indeed, a fit to inelastic neutron-scattering data indicates that there are two one-magnon branches in the vicinity of 180 cm^{-1} at $\mathbf{q} = 0$ [7]. However, while we cannot rule out the possibility that the 2M band in MnV_2O_4 has contributions from one-magnon scattering, our discovery of one-magnon excitations M1 and M2 with linewidths an order of magnitude smaller than that
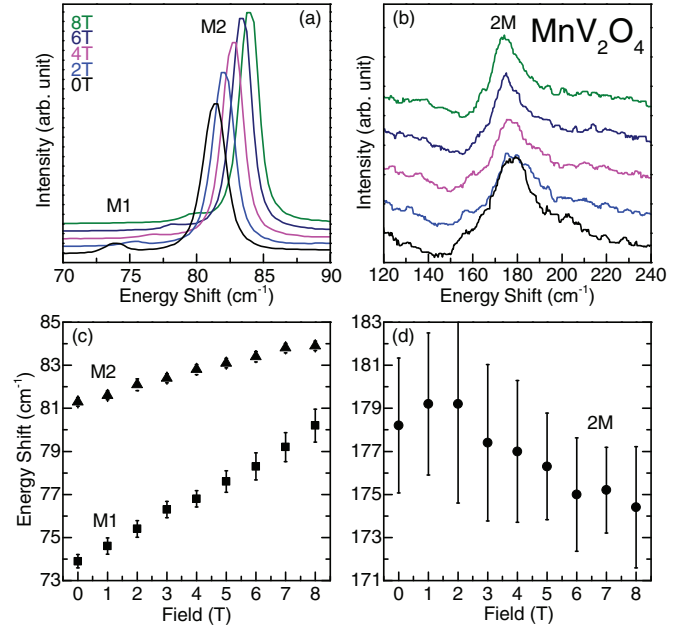

FIG. 2. (Color) (a),(b) Raman-scattering spectra of MnV_2O_4 taken in geometry 1 (see discussion in Sec. II B) at various magnetic fields in the energy ranges (a) 70–90 cm^{-1} and (b) 120–240 cm^{-1}. The data have been offset for clarity. (c),(d) Summaries of the magnetic-field dependences of the peak positions for peaks labeled M1, M2, and 2M, as estimated by eye.

of 2M makes it unlikely that the 2M band in Fig. 1(a) can be attributed to a convolution of two closely spaced one-magnon peaks. It is more likely that the 2M band is associated with two-magnon scattering, involving the excitation of magnon pairs with momenta $+\mathbf{q}$ and $-\mathbf{q}$. The substantially larger linewidth of 2M relative to M1 and M2 reflects the fact that the two-magnon scattering response is governed by the two-magnon density of states.

Interestingly, the temperature dependence of the two-magnon response in MnV_2O_4 is anomalous, as its energy *increases* with increasing temperature toward T_N (see Fig. 1). By contrast, the two-magnon scattering energy in magnetic materials is normally expected to decrease with increasing temperature toward T_N [27], reflecting a decrease in the one-magnon energies and spin-spin correlations with increasing temperature. As discussed below, we propose that the anomalous temperature dependence of the two-magnon scattering response in MnV_2O_4 is indicative of strong spin-lattice coupling associated with zone-boundary magnons.

Figure 3 shows the temperature dependence of the Mn_3O_4 Raman spectrum in the 40–200-cm^{-1} energy range. The higher-frequency Raman spectrum of Mn_3O_4, which is dominated by phonons, was reported by Kim *et al.* [20,21], and will not be reproduced or discussed here. The sharp peak labeled P persists to room temperature and is assigned to a phonon mode. For temperatures near and above T_N, the Raman spectrum of Mn_3O_4 exhibits a broad continuum background similar to that observed in MnV_2O_4. Again, as Mn_3O_4 is insulating [30], we attribute this background to inelastic magnetic, rather than electronic, scattering. For temperatures $T < T_N$, the magnetic continuum background response is suppressed, and several
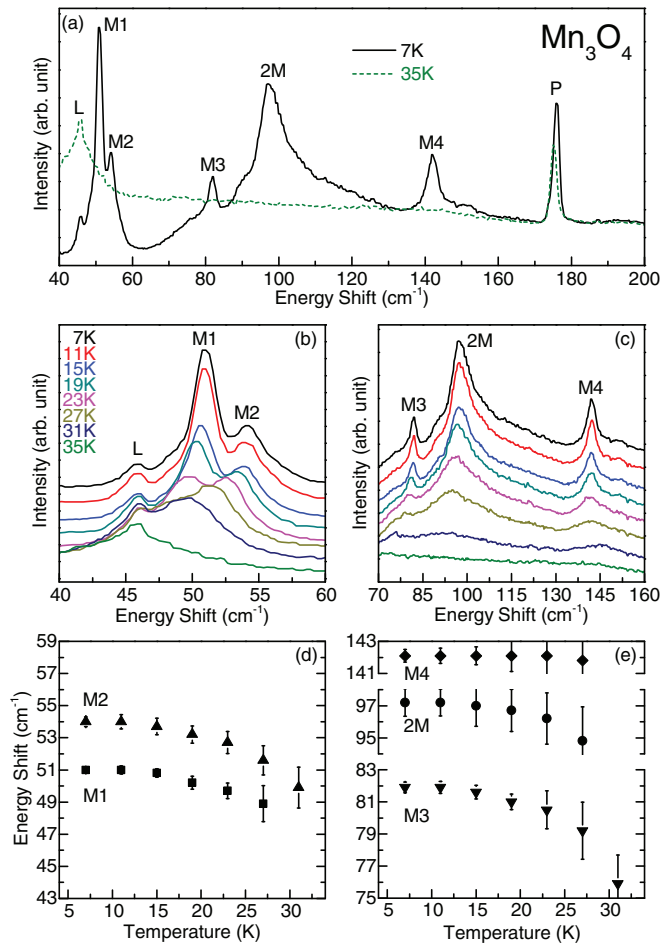
FIG. 3. (Color) (a)–(c) Raman-scattering spectra of Mn_3O_4 at various temperatures in the energy ranges (a) 40–200 cm^{-1}, (b) 40–60 cm^{-1}, and (c) 70–160 cm^{-1}. The data in (b) and (c) have been offset for clarity. (d),(e) Summaries of the temperature dependences of the peak positions for peaks labeled M1–M4 and 2M, as estimated by eye.

FIG. 4. (Color) (a),(b) Raman-scattering spectra of Mn_3O_4 at various magnetic fields in the energy ranges (a) 40–60 cm^{-1} and (b) 70–160 cm^{-1}. The data have been offset for clarity. (c),(d) Summaries of the magnetic-field dependences of the peak positions for peaks labeled M1–M4 and 2M, as estimated by eye.

peaks develop: Four narrow peaks at 51 cm^{-1} (M1), 54 cm^{-1} (M2), 82 cm^{-1} (M3), and 142 cm^{-1} (M4), and a broad asymmetric band at 97.5 cm^{-1} (2M). The weak feature labeled L is an artifact caused by stray light and will not be discussed further.[4]

We identify the four narrow peaks M1–M4 as $\mathbf{q} = 0$ one-magnon excitations, based upon the same criteria discussed above for MnV_2O_4: All of these peaks, except M4, broaden and decrease in energy as $T \rightarrow T_N$. Additionally, the energies of the $\mathbf{q} = 0$ one-magnon modes M1–M4 in Fig. 3 correspond well with the $\mathbf{q} = 0$ magnon energies reported in a previous inelastic neutron-scattering study [7].

Figure 4 shows the magnetic-field dependences of the one-magnon excitations M1–M4 in Mn_3O_4 for a magnetic field

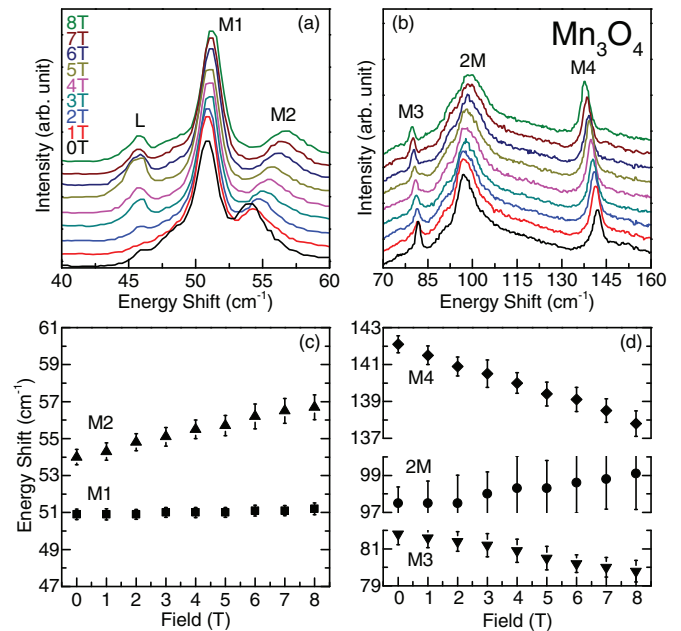applied orthogonal to the net magnetization direction.[5] All peaks except M1 exhibit linear magnetic-field dependences, with M2 increasing in energy at a rate $\Delta E / \Delta H = +0.34$ cm^{-1}/T and M3 and M4 decreasing in energy at rates $\Delta E / \Delta H = -0.25$ and -0.54 cm^{-1}/T, respectively. These field dependences are consistent with earlier claims [7] that the one-magnon excitations identified as M3 and M4 [see Fig. 3(a)] involve spin excitations associated with the frustrated B-site sublattice, as the Mn^{3+} spins on the B site are reported to have an antiferromagnetic component in the direction of the applied magnetic field [5].

We identify the broad two-magnon band 2M in Mn_3O_4 [see Figs. 3(a), 3(c), and 3(e)] as two-magnon scattering. The temperature dependence of this response is similar to that of the one-magnon excitations in Mn_3O_4, but like the two-magnon band observed in MnV_2O_4 (peak 2M in Fig. 1) the linewidth of peak 2M in Mn_3O_4 is much broader than the one-magnon excitations. The broad linewidth of peak 2M is consistent with the fact that the two-magnon scattering response reflects the two-magnon density of states [27]. On the other hand, in contrast to the temperature dependence of the two-magnon scattering response in MnV_2O_4, the two-magnon response 2M in Mn_3O_4 exhibits a conventional temperature dependence, decreasing in energy as $T \rightarrow T_N$ [see Figs. 3(a), 3(c), and 3(e)].

---

[4]The apparent broadening of L at 35 K is simply an artifact caused by the softening of magnetic excitations M1 and M2.

[5]Modes M1–M4 are also sensitive to a magnetic field applied in the ab plane where the net magnetization resides. This field-dependent behavior is more complicated and will be discussed in a paper that examines the complete field dependence of the Raman spectra in Mn_3O_4 and MnV_2O_4.

IV. DISCUSSION

The Raman spectra of both MnV_2O_4 (Fig. 1) and Mn_3O_4 (Fig. 3) exhibit well-defined one- and two-magnon excitations that evolve below T_N from a broad continuum background. This continuum scattering is likely associated with scattering from short-range spin correlations on the frustrated pyrochlore (*B*-site) sublattice. This conclusion is supported by the observation of short-range Mn^{3+} spin correlations above T_N in diffuse neutron-scattering and specific-heat measurements of Mn_3O_4 [31]. Notably, the spin continuum scattering near and above T_N is significantly more prominent in Mn_3O_4 (Fig. 3) than in MnV_2O_4 (Fig. 1). This may reflect the much weaker *B*-site interchain exchange coupling reported in Mn_3O_4 relative to MnV_2O_4 [7], since spin fluctuations are expected to be enhanced in one-dimensional chain systems [25].

The primitive unit cells of Mn_3O_4 and MnV_2O_4 contain six magnetic ions [5,10], and their spin-wave dispersions consist of six branches [7,14]. In Mn_3O_4, we observe four one-magnon excitations at $\mathbf{q} = 0$ whose energies are consistent with zone center magnon energies measured previously with inelastic neutron scattering [7]. In MnV_2O_4, on the other hand, we observe two one-magnon excitations. We do not necessarily expect to observe all six magnetic excitations in either material with Raman scattering, as the particular symmetry of an excitation may be inaccessible to our technique. Even if a magnetic excitation in a given material has a Raman-allowed symmetry, the modulation of the crystal's electronic susceptibility by this excitation may be small, leading to a weak signal. If this is the case, our observation of fewer one-magnon excitations in MnV_2O_4 than in Mn_3O_4 may reflect the difference between the orbital configurations of the V^{3+} and Mn^{3+} ions.

Significantly, while Chung *et al.* [7] report a single $\mathbf{q} = 0$ magnon near 80 cm^{-1} in MnV_2O_4, we observe two $\mathbf{q} = 0$ magnons at 74 and 81 cm^{-1} in this material. One possible explanation for this discrepancy is that the two modes we observe are associated with a slight splitting of two transverse magnon branches at $\mathbf{q} = 0$—which is not resolved by Chung *et al.*—due to anisotropy effects in MnV_2O_4. However, a more likely interpretation is that the 74- and 81-cm^{-1} modes we observe in MnV_2O_4 are associated with a pair of one-magnon branches that were recently reported by Magee to exhibit a crossing at a momentum transfer equivalent to $\mathbf{q} = 0$ in MnV_2O_4 [28]. This is consistent with the *number* of magnon modes we observe in this energy range; importantly, however, we measure an 8-cm^{-1} (1-meV) splitting between the single-magnon modes, rather than a band crossing, at $\mathbf{q} = 0$ in MnV_2O_4.

The $\mathbf{q} = 0$ one-magnon spectrum of MnV_2O_4 we observe (see Fig. 1) should put constraints on the orbital ground state of this material. To clarify this point, note that there are currently several proposed orbital ordering schemes for the V^{3+} ion in MnV_2O_4 [13–19]. Since each orbital configuration has a different electron overlap, and thus different exchange parameters, a principal test of the orbital order in MnV_2O_4 has been a comparison between exchange parameters calculated from particular orbital configurations (e.g., [14] and [19]) and exchange parameters extracted from a fit to inelastic neutron-scatting data reported by Chung *et al.* [7]. However,

this fit does not account for our observation of two $\mathbf{q} = 0$ magnon excitations near 80 cm^{-1} in MnV_2O_4. Specifically, to explain the two $\mathbf{q} = 0$ magnon excitations near 80 cm^{-1}, one of the four higher-energy bands at the zone center of the fit given by Chung *et al.* would have to be lowered by at least 8 meV. More recent higher-resolution neutron-scattering measurements by Magee show that one of the higher-energy magnon branches in MnV_2O_4 does indeed disperse downward near the zone center; however, the Magee neutron study reports a crossing of magnon branches near 80 cm^{-1} at $\mathbf{q} = 0$ rather than the 8-cm^{-1} splitting between $\mathbf{q} = 0$ magnon modes that we observe [28]. In short, the $\mathbf{q} = 0$ magnon spectrum we measure in MnV_2O_4 indicates that a revised fit to magnon dispersion data is needed to obtain improved estimates of the exchange parameters and orbital ground state in MnV_2O_4.

The two-magnon scattering responses at 178 cm^{-1} in MnV_2O_4 (Fig. 1) and 98 cm^{-1} in Mn_3O_4 (Fig. 3) represent the creation of pairs of spin waves with momenta $+\mathbf{q}$ and $-\mathbf{q}$. The temperature dependence of the two-magnon scattering energy ω_{2M} has been calculated by numerous authors [27,32,33]: ω_{2M} is expected to increase with decreasing temperature, following the temperature dependence of the one-magnon energy. The temperature dependence of the two-magnon response in MnV_2O_4 is anomalous, as the two-magnon energy *decreases* with decreasing temperature [see Fig. 1(c) and 1(f)].

The two-magnon scattering intensity is proportional to the two-magnon density of states and is thus dominated by pairs of spin waves with momenta near the edge of the Brillouin zone. Therefore, the anomalous two-magnon temperature dependence in MnV_2O_4 must be associated with magnon interaction effects at the zone boundary. Strong spin-lattice coupling associated with the zone-boundary magnons in MnV_2O_4 is the simplest and most likely explanation for the anomalous two-magnon temperature dependence, particularly given the evidence for strong spin-lattice coupling apparent in the closely spaced magnetic and structural phase transitions of MnV_2O_4. A similar temperature dependence of the two-magnon band in the spin-dimer system $TlCuCl_3$ was also observed and attributed to strong spin-phonon coupling [34].

Notably, there is no evidence for anomalies associated with either of the $\mathbf{q} = 0$ one-magnon peaks M1 and M2 in MnV_2O_4. These $\mathbf{q} = 0$ magnon modes are well separated in energy from—and hence are not expected to mix with—the $\mathbf{q} = 0$ phonon modes of MnV_2O_4 [23,35]. Strong spin-lattice coupling should be more pronounced near the Brillouin-zone boundary in this material, where the dispersed acoustic phonons (or possibly softened optical phonons) are more likely to overlap in energy with magnons.

Our Raman results motivate a more conclusive investigation of possible mixing of the spin and lattice degrees of freedom at the zone boundary in MnV_2O_4, particularly an inelastic neutron-scattering search for anomalies in the temperature dependence of zone-boundary magnons and phonons in the 9–12-meV range. For example, neutron-scattering studies of the manganese perovskites revealed spin-wave softening and linewidth broadening of the zone-boundary magnons caused by spin-phonon coupling [36].

In Mn_3O_4, we did not find a similar anomalous temperature dependence for any of the magnetic excitations we were able to observe. Spin-lattice coupling is known to have significant

effects in Mn_3O_4 [20,21,37–40], which raises the question of why we do not observe magnon anomalies in Mn_3O_4 similar to that observed in MnV_2O_4. A likely reason for this discrepancy is simply that magnon-phonon coupling in Mn_3O_4 occurs in a region of the Brillouin zone that is inaccessible to Raman scattering. Temperature-dependent neutron-scattering studies, which would allow a study of magnon and phonon anomalies throughout the Brillouin zone of Mn_3O_4, are needed to provide a more comprehensive search for magnon anomalies associated with strong spin-lattice coupling.

V. SUMMARY

In summary, we have measured the temperature and magnetic-field dependences of one- and two-magnon excitations in the magnetically frustrated spinels MnV_2O_4 and Mn_3O_4. Both materials exhibit diffusive spin scattering above T_N, which we associate with incoherent spin fluctuations on the B-site sublattice. Below T_N, one- and two-magnon excitations develop in both MnV_2O_4 and Mn_3O_4. In Mn_3O_4, the zone center magnon spectrum we observe matches well with previous neutron-scattering results and spin-wave calculations. However, in MnV_2O_4, we observe a pair of zone center magnon modes near 80 cm^{-1}, one of which is not predicted by either current spin-wave calculations or the fit

to inelastic neutron-scattering data of Chung *et al.* [7]. The $\mathbf{q} = 0$ magnon results on MnV_2O_4 presented here, along with more recent neutron-scattering measurements of the magnon branches in MnV_2O_4 by Magee [28], indicate that a revised fit to the magnon dispersion data for MnV_2O_4 is needed to obtain improved estimates of the exchange parameters and orbital ground state in MnV_2O_4. Finally, we show that the two-magnon energy of Mn_3O_4 exhibits a conventional temperature dependence, but that the two-magnon energy of MnV_2O_4 shows an anomalous softening with decreasing temperature below T_N. We propose that this softening reflects strong coupling between vibrational and magnetic excitations near the zone boundary in MnV_2O_4, and we suggest that high-resolution neutron-scattering studies of zone-boundary magnons and/or phonons are needed to further elucidate the nature of this strong spin-phonon coupling.

[1] S.-H. Lee, H. Takagi, D. Louca, M. Matsuda, S. Ji, H. Ueda, Y. Ueda, T. Katsufuji, J.-H. Chung, S. Park, S.-W. Cheong, and C. Broholm, J. Phys. Soc. Jpn. **79**, 011004 (2010).

[2] R. McCallum, D. Johnston, C. Luengo, and M. Maple, J. Low Temp. Phys. **25**, 177 (1976).

[3] A. Irizawa, S. Suga, G. Isoyama, K. Shimai, K. Sato, K. Iizuka, T. Nanba, A. Higashiya, S. Niitaka, and H. Takagi, Phys. Rev. B **84**, 235116 (2011).

[4] M. Kopeć, J. R. Dygas, F. Krok, A. Mauger, F. Gendron, B. Jaszczak-Figiel, A. Gagor, K. Zaghib, and C. M. Julien, Chem. Mater. **21**, 2525 (2009).

[5] G. B. Jensen and O. V. Nielsen, J. Phys. C **7**, 409 (1974).

[6] B. Chardon and F. Vigneron, J. Magn. Magn. Mater. **58**, 128 (1986).

[7] J.-H. Chung, J.-H. Kim, S.-H. Lee, T. J. Sato, T. Suzuki, M. Katsumura, and T. Katsufuji, Phys. Rev. B **77**, 054412 (2008).

[8] H. D. Zhou, J. Lu, and C. R. Wiebe, Phys. Rev. B **76**, 174403 (2007).

[9] T. Suzuki, M. Katsumura, K. Taniguchi, T. Arima, and T. Katsufuji, Phys. Rev. Lett. **98**, 127203 (2007).

[10] V. O. Garlea, R. Jin, D. Mandrus, B. Roessli, Q. Huang, M. Miller, A. J. Schultz, and S. E. Nagler, Phys. Rev. Lett. **100**, 066404 (2008).

[11] Y. Nii, H. Sagayama, H. Umetsu, N. Abe, K. Taniguchi, and T. Arima, Phys. Rev. B **87**, 195115 (2013).

[12] Y. Huang, Z. Qu, and Y. Zhang, J. Magn. Magn. Mater. **323**, 970 (2011).

[13] H. Tsunetsugu and Y. Motome, Phys. Rev. B **68**, 060405 (2003).

[14] R. Nanguneri and S. Y. Savrasov, Phys. Rev. B **86**, 085138 (2012).

[15] O. Tchernyshyov, Phys. Rev. Lett. **93**, 157206 (2004).

[16] D. I. Khomskii and T. Mizokawa, Phys. Rev. Lett. **94**, 156402 (2005).

[17] G.-W. Chern, N. Perkins, and Z. Hao, Phys. Rev. B **81**, 125127 (2010).

[18] T. Katsufuji, T. Takubo, and T. Suzuki, Phys. Rev. B **87**, 054424 (2013).

[19] S. Sarkar, T. Maitra, R. Valentí, and T. Saha-Dasgupta, Phys. Rev. Lett. **102**, 216405 (2009).

[20] M. Kim, X. M. Chen, Y. I. Joe, E. Fradkin, P. Abbamonte, and S. L. Cooper, Phys. Rev. Lett. **104**, 136402 (2010).

[21] M. Kim, X. M. Chen, X. Wang, C. S. Nelson, R. Budakian, P. Abbamonte, and S. L. Cooper, Phys. Rev. B **84**, 174424 (2011).

[22] M. Kim, Ph.D. thesis, University of Illinois at Urbana-Champaign, 2011.

[23] K. Takubo, R. Kubota, T. Suzuki, T. Kanzaki, S. Miyahara, N. Furukawa, and T. Katsufuji, Phys. Rev. B **84**, 094406 (2011).

[24] Y. Nii, N. Abe, K. Taniguchi, and T. Arima, Appl. Phys. Lett. **100**, 051905 (2012).

[25] P. Lemmens, G. Güntherodt, and C. Gros, Phys. Rep. **375**, 1 (2003).

[26] K.-Y. Choi, P. Lemmens, P. Scheib, V. Gnezdilov, Y. G. Pashkevich, J. Hemberger, A. Loidl, and V. Tsurkan, J. Phys. Condens. Matter **19**, 145260 (2007).

[27] M. Cottam and D. Lockwood, *Light Scattering in Magnetic Solids* (Wiley, New York, 1986).

[28] A. J. Magee, Ph.D. thesis, Royal Holloway, University of London, 2010.

[29] S. Miyahara, K. Takubo, T. Suzuki, T. Katsufuji, and N. Furukawa, arXiv:1012.4073.

[30] A. West, *Solid State Chemistry and its Applications* (Wiley, New York, 1985).

[31] A. Kuriki, Y. Moritomo, S. Xu, K. Ohoyama, K. Kato, and A. Nakamura, J. Phys. Soc. Jpn. **72**, 458 (2003).

[32] J. Sólyom, Zeitschrift für Physik **243**, 382 (1971).

[33] M. Cottam, Solid State Commun. **11**, 889 (1972).

[34] K.-Y. Choi, G. Güntherodt, A. Oosawa, H. Tanaka, and P. Lemmens, Phys. Rev. B **68**, 174412 (2003).

[35] K. Myung-Whun, S. Y. Jang, T. Katsufuji, and A. V. Boris, Phys. Rev. B **85**, 224423 (2012).

[36] P. Dai, H. Y. Hwang, J. Zhang, J. A. Fernandez-Baca, S.-W. Cheong, C. Kloc, Y. Tomioka, and Y. Tokura, Phys. Rev. B **61**, 9553 (2000).

[37] J. Chung and K. Lee, J. Phys. Soc. Jpn. **82**, 034707 (2013).

[38] T. Suzuki and T. Katsufuji, Phys. Rev. B **77**, 220402 (2008).

[39] R. Tackett, G. Lawes, B. C. Melot, M. Grossman, E. S. Toberer, and R. Seshadri, Phys. Rev. B **76**, 024409 (2007).

[40] T. Suzuki, K. Adachi, and T. Katsufuji, Journal of Physics: Conference Series **31**, 235 (2006).

[41] S.-H. Baek, N. J. Curro, K.-Y. Choi, A. P. Reyes, P. L. Kuhns, H. D. Zhou, and C. R. Wiebe, Phys. Rev. B **80**, 140406 (2009).